CAPSID PROTEINS ARE NECESSARY FOR REPLICATION OF A DENSOVIRUS

Deborah Garcia, Doriane Mutuel, Mylène Ogliastro, Guillaume Cambray

CAPSID PROTEINS ARE NECESSARY FOR REPLICATION OF A DENSOVIRUS

Deborah Garcia[1], Doriane Mutuel[1], Mylène Ogliastro[1] and Guillaume Cambray[1,2,*]

[1] Diversité des Génomes et Interactions Microorganismes Insectes (DGIMI), UMR 1333, Univ Montpellier, INRA, 34095 Montpellier, France

[2] Centre de Biochimie Structurale (CBS), UMR 5048, Univ Montpellier, CNRS, 34090 Montpellier, France

[*] To whom correspondence should be addressed. Tel: +33 6 08 86 06 89; Email: cambray.guillaume@gmail.com

Present Address: Centre de Biochimie Structurale, CNRS UMR 5048 - UM - INSERM U 1054, 29 rue de Navacelles 34090, MONTPELLIER, France

ABSTRACT

Despite tight genetic compression, viral genomes are often organized in functional gene clusters, a modular structure that might favor their evolvability. This has greatly facilitated biotechnological developments, such as the recombinant Adeno-Associated Virus (AAV) systems for gene therapy. Following this lead, we endeavored to engineer the related insect parvovirus *Junonia coenia* densovirus (JcDV) to create addressable vectors for insect pest biocontrol. To enable safer manipulation of capsid mutants, we translocated the non-structural (*ns*) gene cluster outside the viral genome. To our dismay, this yielded a virtually non-replicable clone. We linked the replication defect to an unexpected modularity breach, as *ns* translocation truncated the overlapping 3' UTR of the capsid transcript (*vp*). We found that native *vp* 3'UTR is necessary to high VP production, but that decreased expression do not adversely impact the expression of NS proteins, which are known replication effectors. As nonsense *vp* mutations recapitulate the replication defect, VP proteins appear directly implicated in the replication process. Our findings suggest intricate replication-encapsidation couplings that favor maintenance of genetic integrity. We discuss possible connections with an intriguing cis-packaging phenomenon previously observed in parvoviruses, whereby capsids preferentially package the genome from which they were expressed.

IMPORTANCE

Densoviruses could be used as biological control agents to manage insect pests. Such applications require in depth biological understanding and associated molecular tools. However, the genomes of these viruses remain hard to manipulate due too poorly tractable secondary structures at their extremities. We devised a construction strategy that enable precise and efficient molecular modifications. Using this approach, we endeavored to create a split clone of the Junonia coenia densovirus (JcDV) that can be used to safely study the impact of capsid mutations on host specificity. Our original construct proved to be non-functional. Fixing this defect led us to uncover that capsid proteins and their correct expression are essential for viral replication. This points to an intriguing link between replication and packaging, which might be shared we related viruses. This serendipitous discovery illustrates the power of synthetic biology approaches to advance our knowledge of biological systems.

INTRODUCTION

Viruses represent the most diverse and abundant biological entities on earth and can be found in nearly all organisms. Over the last decade, it has become increasingly apparent that the evolutionary success of viruses is largely supported by their propensity to recombine (1). As if to promote evolvability, the genome of many viruses displays modular architecture, wherein sequences involved with capsid formation and those coding for replicative functions are segregated in distinct functional blocks.

Such modularity is clearly apparent in *Parvoviridae*. Member of this family are characterized by single stranded DNA genomes of 4-6kb that invariably consist in similarly sized *vp* and *ns* gene clusters, flanked by telomeric sequences. The *vp* (viral particle) block bears 1-3 sequence coding for an icosahedral capsid (T=1), while the *ns* (non-structural) block code for 1-4 proteins involved in replication, packaging and other often undefined functions. Telomeric sequences can fold into hairpins involved in replication and also contain packaging signals. This modular organization has been exploited in the context of gene therapy to, for example, produce pseudotyped recombinant AAV virions based on telomeres, *ns* and *vp* genes from different parvoviruses (2).

In this work, we wanted to physically dissociate the *vp* and *ns* gene clusters to generate a non-propagatable clone of the Junonia Coenia Densovirus (JcDV).

JcDV is the type member of the genus *Ambidensovirus*, which comprises invertebrate parvoviruses characterized by tail to tail orientation of their *ns* and *vp* blocks (Figure 1A). This original architecture usually results in a 60 nts overlap between the 3'UTR of their respective transcripts. JcDV can be pathogenic for several species of insects from the Lepidoptera order, including agriculturally relevant pests such as the Fall Army Worm (*Spodoptera frugiperda*), a polyphagous crop pest that is currently spreading over the worlwd at alarming rates {Matthews:2018ee}. Densoviruses have long been considered promising candidates for the biological control of insect populations, and several field trials have confirmed there potential efficacies (3, 4).

In this perspective, the ability to fine tune host tropism would be particularly desirable to establish precise and controllable biocontrol solutions. As with other vertebrate parvoviruses (5, 6), the variation of few amino-acid residues at the surface of JcDV's capsid have been shown to modulate JcDV's host range (7). To better understand—and eventually control—these sequence determinants, we endeavored to develop a high-throughput screen of rationally engineered capsid variants in which the link between mutations and consequent capsid performances is established by deep sequencing of mutated *vp* genes packaged in their cognate capsid (8-10). Concerned with potential biohazards, we first wished to establish a non-propagatable system wherein mutant virions could be screened for capsid functionality, while not being capable of effecting further productive infection and transmission.

To produce non-propagatable virions that can nonetheless package the *vp* gene required for subsequent sequencing-based capsid identification, we moved the *ns* gene block in *trans* and replaced it by a reporter gene block of the same size. Although similar manipulation had been successfully accomplished for several parvoviruses, ours yielded a completely nonfunctional JcDV clone. Subsequent investigation led us to link the alteration of *vp* transcript's 3'UTR to a stark decrease in VP protein production and a near complete shutdown of viral replication. This allowed us to unveil a direct and essential involvement of the VP proteins in the replication process of a parvovirus.

MATERIAL AND METHODS

Plasmid constructions

All enzymes were purchased from NEB. Phusion Hot-Start Flex polymerase (NEB) was used for all PCR reactions. NEB Turbo cells were used for transformation of all constructs, except construct comprising ITRs, which were transformed in NEB stable strain and grown at 30°C to improve stability. Primers were ordered from IDT. Constructions were systematically verified by Sanger sequencing (Eurogentec). Constructions assayed in this work are listed in Table 1. A more exhaustive plasmid list including construction intermediates described below is provided in Supplementary Table 1. Oligonucleotides are listed in Supplementary Table 2.

Construction of JcDV clones. The WT JcDV clone (p14) was derived from the published pBRJH clone (11) by outcloning the *cat* cassette (conferring resistance to chloramphenicol) from the pSB1C3 of p10 in place of the *bla* cassette (conferring resistance to ampicillin) upon BspHI digest. Non-propagatable vectors were constructed using Golden Gate cloning (12) of several fragments to avoid problematic PCR amplification of unstable ITRs. A graphical overview is presented in Supplementary Figure 1. Fragments were flanked by BsaI sites to eventually enable directed and seamless cloning and initially subcloned into a minimal donor backbone comprising a p15a origin of replication and chloramphenicol resistance (pBbA2c-RFP, 13) modified to contain matching BsaI sites. An extended version of JcDV's ITR (14) was synthesized (Genewiz, p39) and subcloned into the donor vector amplified by o122+o147 to yield p47. The P93 promoter was amplified from p14 (o114+115) and cloned into the donor vector amplified by o127+o128 to yield p46. A reporter block comprised of eGFP, actin promoter A3 from *Bombyx mori* and a neomycin resistance gene (*neo*) was constructed by assembly PCR. eGFP and PA3 were separately amplified from pITR-A3-GFP (11) using o54+o6 and o7+o8, respectively. The *neo* gene was amplified from pNEO (Amersham) using o9+o55. The 3 amplicons were assembled using o54+o55 and cloned into the donor vector amplified by o56+o57 to yield p17. eGFP was then substituted by mVenus: p17 was amplified with o63+o64; mVenus was amplified from plasmid mCerulean3-mVenus-FRET-10 (a gift from Michael Davidson, Addgene plasmid # 58180) using o61+o62; and the two amplicons were cloned at BsmBI sites introduced during the PCRs to yield p36. The sequence

corresponding to P9-vp123 (*i.e.* excluding the *vp4* part) was amplified from p14 using o114+o94 and cloned into the donor backbone amplified with o85+127 to yield p42. In this process, a double BsmBI site was introduced to enable subsequent in-frame cloning of *vp4*. The latter was amplified from p14 using o96+o97 and cloned into the donor backbone amplified with o116+o117 to yield p40. Unlike other donor constructs, *vp4* in p40 is flanked by BsmBI sites.

To construct the acceptor plasmid, we first cloned the *ns* gene block under the control of a strong OpEI-2 baculoviral promoter in a pIZ backbone. For this, we amplified the *ns* gene block using an assembly PCR designed to remove a BsaI site in *ns3* through the introduction of a silent Arg substitution (AGG119AGA). The two *ns* fragments were amplified from p14 using o112+o19 and o113+o20, assembled using o112+113 and cloned between BamHI and AgeI sites of p25 (pIZ-Flag6His-Siwi, 15) to yield p45. A landing pad comprised of two BsaI sites was assembled by annealing o120+o121 and cloned at the BspHI site of p45 to yield p49.

Donor vectors p47 (ITR), p46 (P93), p36 (mVenus-A3-neo) and p42 (P9-vp123-2xBsmBI) and acceptor vector p49 were used in a one-pot Golden Gate reaction with BsaI to yield the *vp4*-less intermediate p57. The defective non-propagatable clone p58 was constructed by Golden Gate cloning of p40 into p57 using BsmBI.

To construct amended versions of the defect clone, longer versions of p40 that extend the sequence 3' of vp4 were amplified from p14 using o243+o239 and o243+244 and cloned into the donor backbone amplified by o116+o117 to yield p105 and p106, respectively. These were introduced in p57 by Golden Gate cloning (BsmBI) to yield the non-propagatable clones p103 and p104, respectively, both of which functioning as originally intended.

Targeted mutations in *vp4* were introduce by site-directed mutagenesis of p105 using o393+o394 and o395+o396 to yield p252 and p253, respectively. Golden Gate cloning of the latter plasmids in p57, yielded p254 and p255, respectively.

Construction and modification of gene block plasmids. Plasmid p92, p90 and p91 have been published previously under the names pJA (16), pJΔVP and pJΔNS (17), respectively. Plasmid p91 served to produce p93 and p118 by site-directed mutagenesis, using o223+o227 and o223+o285, respectively. The same strategy was used to introduce 7m and 12m mutations in p90 (p91) with o295+o296 and o297+o298, yielding p146 and p147, respectively (p144 and p145).

Construction of a replication reporter. AgeI and SacI were used to digest p58 and pFAB217 (18). The p58 reaction products were dephosphorylated using antarctic phosphatase and ligated to pFAB217's fragments using T4 DNA ligase to yield p73, in which the *ns* gene block is replaced by a small ~500 nts fragment of non-functional DNA. The PA3-eGFP cassette from pITR-A3-GFP (11) was amplified with o233+234. A large non-functional DNA fragment was amplified from pGC4783 (19) using o235+o236. These two amplicons were assembled by PCR using o233+o236, previously phosphorylated with T4 PNK. The resulting amplicon was cloned at the BbsI sites of p73. This yielded p116, in which a reporter fragment of the same length of the original JcDV sequence is flanked by promoter-less ITRs.

Cell line and transfection

The insect cell line Ld652Y (20) was maintained at 28°C in TC100 medium (Lonza) supplemented with 10% heat-inactivated fetal calf serum (Thermo scientific), and antibiotic/antimytotic cocktail (10 units/mL penicillin, 10 µg/mL streptomycin and 25 fg/mL Amphotericin B, Gibco). Ld652Y cells were originally derived from *Lymantria dispar* ovaries and have been found to be most sensitive to JcDV infection (16). Flask-grown cells at ~70% confluence were harvested, seeded on 24-well plates (10^5 cells/well) and cultured overnight. Cells were then transfected with plasmids DNA (250 ng per plasmid per well) using FuGENE HD (Promega, 1:8 ratio), and cultured at 28°C. The culture medium was changed to a fresh one without transfection material 16h after transfection.

Quantification of replication efficiency by qPCR

Transfected cells were resuspended in PBS at either 16h or 72h post-transfection and frozen in microtubes at -80C. Samples were lyzed through three freeze-thaw cycles (-80C/+20C) and clarified at 10,000 rpm for 10 minutes. For each sample, supernatants were diluted 100-fold in TE and 2.5 uL were directly used as templates in 10 uL qPCR reactions, using SYBR Green qPCR mix (Bioline) on a LightCycler 480 instrument (Roche). Each sample was assayed in technical triplicate, and their average used for further calculations. Primers o182+o183 (*neo*) were used to specifically quantify replication of the rearranged non-propagatable genomes, with a hybridization temperature of 54°C. Primers o307+308 (eGFP) were used to quantify the replication reporter p116, with a hybridization temperature of 60°C. The following amplification parameters were

used: 2 min at 50°C and 2 min at 95°C, followed by 40 cycles each consisting of 15 s at 95°C and 30 s at the adequate hybridization temperature. Data were analysed with LightCycler 480 software (version 1.5). Standard curves were generated after 40 cycles using ten 2-fold serial dilutions of p58 or p116. In each case, a linear range was obtained over the eleven standard points, enabling calculation of viral DNA copy number. Three biological replicates were performed for each assay.

Quantification of transcript abundance by RT-qPCR

Total RNA was extracted from cells 12h post-transfection using the RNeasy Mini kit (Qiagen). RNA samples were treated with Turbo DNAse (Ambion) and cDNAs were synthesized from polyA tails using SuperScript III reverse transcriptase (Invitrogen). Transcript abundances were measured with o40+o41 and o365+o366, which respectively binds to *vp4* and *ns1*, as described previously (17, 21). Cellular β-actin was used to control for RNA degradation and other potential sample to sample variations, as previously described (17). Each sample was assayed in technical triplicate and their average used for further calculations. Three biological replicates were performed.

3'RACE assays

Total RNA was extracted from cells 72h post-transfection using the RNeasy Mini kit (Qiagen). We used 5'/3' RACE Kit, 2nd Generation (Roche) according to the manufacturer's instructions. To specifically target *vp* transcripts we used primers o40 and o37 for the first and second round of PCR, respectively. Amplicons were Sanger-sequenced using o37. Chromatographs were plotted using ApE (v2.0.61).

Quantification of protein abundance by immunofluorescence microscopy

Cells were transfected as described above and fixed 96h post-transfection with 4% paraformaldehyde for 20 min. Cells were washed twice in PBS and permeabilized with PBS+0.1% Triton (PBT). Blocking was performed with PBT+1%BSA for 1 hour. Cells were incubated with appropriate primary antibodies with PBT+0.1% BSA for 1 h, as described previously (17). Samples were washed twice in PBS and incubated overnight at 4°C in PBS. Samples were then incubated for 1h with anti-rabbit Alexa Fluor 568 secondary antibodies (Molecular Probes-Invitrogen) diluted at 1:500. Nuclei were labeled for 20 min with Hoechst 33342 (Sigma).

Brightfield and fluorescence images were automatically acquired using a Cellomics platform equipped with 349 and 540 nm LED, Hoechst and Cy3 filter cube sets, a 10X Plan Apochromat 0.45NA objective and ORCA ER Hamamatsu digital camera. Images were batched processed with the Cellomics Studio software. Cell nuclei were automatically segmented using Hoechst signal. Abnormal signals were excluded to avoid artefacts. Mean Alexa Fluor 568 fluorescence signal per pixel in the segmented areas was computed for each cell in each sample.

Western blots

Cells were seeded in 6-well plates (5.10^5 cells/well), transfected with 1 µg of plasmid DNA and harvested 96h after transfection. Protein concentration was assessed by Bradford analysis, samples were diluted 1:20 and equal amounts of lysates were separated onto 4–15 % gel to run SDS-PAGE. Migrated materials were transferred to PVDF membranes (Immobilon-P, Millipore) for Western blot analysis using and revealed by enhanced chemiluminescence (Luminata Crescendo, Millipore).

Data analysis

GT-content analysis was performed using custom python script and plotted using R. The factorial analysis presented in Figure 3 was performed using the *anova* function in R. Analysis of Cellomics data used custom R scripts. Scripts and data are available upon request to GC.

ID	*Name*	*Description*	*reference*
p14	pBRJH-CmR	WT JcDV clone derived from the original pBRJH clone	This work
p58	NoPropJcDV-venus-vp4-16_tail	Original (defective) design of JcDV's non-propagatable clone with 16 nts after vp's stop codon	This work
p90	pJΔvp	JcDv's P93 and *ns* followed by 484 nts after *ns1*'s stop codon	17
p91	pJΔns	JcDv's P9 and *vp* followed by 115 nts after *vp*'s stop codon	17
p92	pJA	pBRJH derivative with truncated ITRs (no hairpin, no replication)	16

p93	pJΔns_49_tail	JcDv's P9 and *vp* followed by 49 nts after *vp*'s stop codon	This work
p103	NoPropJcDV-venus-vp4-115_tail	Amended (functional) design of JcDV's non-propagatable clone with 115 nts after *vp*'s stop codon	This work
p104	NoPropJcDV-venus-vp4-91_tail	Amended (functional) design of JcDV's non-propagatable clone with 91 nts after *vp*'s stop codon	This work
p116	JcDV_Replication_reporter	JcDV's extended (oxford) ITRs flanking a DNA sequence of the same length as the WT genome. Comprises eGFP driven by *B. Mori*'s A3 promoter and followed by SV40 polyadenylation signal	This work
p118	pJΔns-75_tail	JcDv's P9 and *vp* followed by 75 nts after *vp*'s stop codon (stops just after polyA site)	This work
p144	pJΔns-7m_ns_recod	JcDv's P9 and *vp* followed by 115 nts after *vp*'s stop codon with 7 substitutions in the ns1 overlapping region	This work
p145	pJΔns-12m_ns_recod	JcDv's P9 and vp followed by 115 nts after vp's stop codon with 12 substitutions in the ns1 overlapping region	This work
p146	pJΔvp-7m_ns_recod	JcDv's P93 and ns followed by 484 nts after ns1's stop codon. 7 silent substitutions in the end of ns1	This work
p147	pJΔvp-12m_ns_recod	JcDv's P93 and ns followed by 484 nts after ns1's stop codon. 12 silent substitutions in the end of ns1	This work
p254	NoPropJcDV-venus-vp4_168tag-115_tail	Amended design of JcDV's non-propagatable clone with 115 nts after *vp*'s stop codon and tat542tag substitution in *vp* (stop codon)	This work
p255	NoPropJcDV-venus-vp4_314aa--115_tail	Amended design of JcDV's non-propagatable clone with 115 nts after *vp*'s stop codon and aat687aa- deletion in *vp* (frameshift)	This work

Table 1 – Plasmid used in this work

RESULTS

Translocation of ns gene cluster abolishes replication of the rearranged JcDV genome

In parvoviruses, replication occur through a rolling-hairpin mechanism that involves *ns* gene functions and the terminal hairpins that flank the genome (ITRs; Figure 1A; 22). These telomeric regions are also important for genome packaging . In an effort to construct a safe, non-propagatable variant of a JcDV infectious clone, we replaced the *ns* gene block by a reporter cassette and cloned it under a strong heterologous promoter on the same plasmid, but outside of the viral genome, as delineated by the telomeres (Figure 1B). We expected that, upon transfection, *ns* genes would be expressed at sufficient levels to ensure replication of the modified genome from its telomeres and its subsequent packaging in capsids originating from *vp* genes. To avoid any size-related packaging problem (23), the reporter cassette was designed to be the same size as the translocated *ns* block. Cells transduced by the resulting virions would produce VP proteins, a drug resistance protein and a fluorescence protein, but would not be able to support further replication or packaging in the absence of NS functions (Figure 1D).

The terminal hairpins that flank the genome of parvoviruses are particularly refractory to PCR amplification. This has typically restricted modifications of these genomes to those permitted by available restriction sites. Here, we developed a Golden Gate cloning strategy to enable more precise manipulations, and could effortless and seamlessly assemble the designed plasmid above from individual building blocks (see Materials and Methods and Supplementary Figure 1). This plasmid could be transfected with an efficacy of about 60%, as estimated by counting fluorescent cells 3 days post-transfection (pt). Upon transduction of naïve cells with a supernatant of this culture collected at 7 days pt, we could not observe any fluorescent cell, indicating that the construct did not behave as expected (Supplementary Figure 2). All JcDV proteins for which we possess antibodies (VP, NS1 and NS2) could be qualitatively detected by immunofluorescence upon transfection of the plasmid (data not shown), indicating that the defect did not originate from complete absence of expression. Quantification of viral genome abundance after transfection, however, demonstrated an almost complete absence of replication (Figure 2, top).

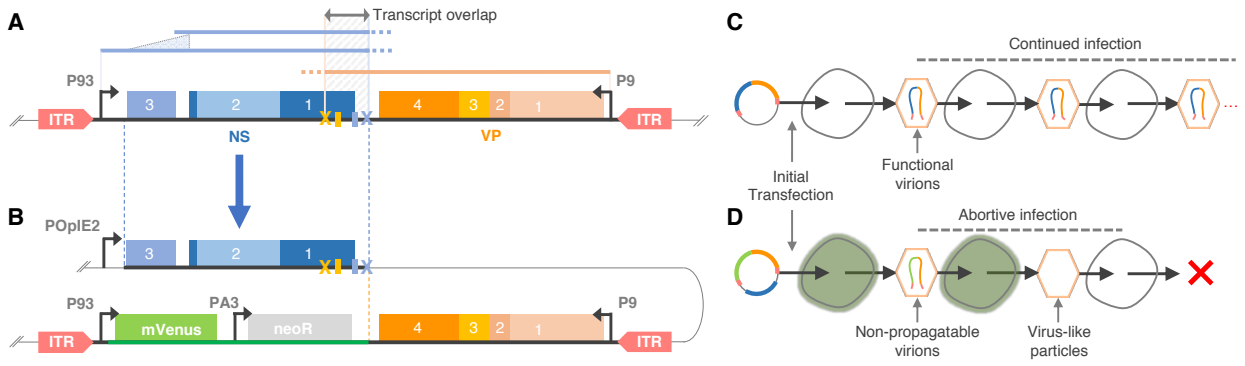

Figure 1 – Initial design for the construction of a non-propagatable JcDV clone.

A. Functional architecture of the infectious JcDV clone. *ns* (blue) and *vp* (orange) gene blocks are in tail to tail orientation. Each produce a single transcript (blue and orange lines) from a promoter partly located in the inverted terminal repeats (ITRs, red). The *ns* transcript is alternatively spliced, as shown. Due to the location of *ns* and *vp* polyadenylation signals and sites (blue and orange small rectangle and cross, respectively), the two transcripts overlap over a complementary region of 60 nucleotides (grey arrow, top). **B.** Architecture of the non-propagatable clone. The *ns* block (start of *ns3* to end of *ns* transcript) was cloned out of the genome under the control of a strong baculovirus promoter, and replaced by a reporter block of the same size comprising the *mVenus* fluorescent protein gene and a neomycin resistance gene. In this process, VP's 3'UTR was truncated by 44 nts to avoid recombination-prone sequence duplication. **C.** Continued infection upon transfection of WT clone. Upon packaging of the WT genome, produced virions can propagate to naïve cells leading to uncontrolled spread of the infection. **D.** Transfection of non-propagatable clones do not permit infection. *Trans* complementation by NS function enable initial genome replication in transfected cells. Upon packaging, genomes devoid of NS functions cannot replicate in naïve cells, containing the spread of the virus.

Complementation assays link replication defect to vp gene

As NS proteins are involved in replication, we reasoned that the translocation of the *ns* block could negatively impact its expression pattern. We expected that viral genes moved outside of the genome would experience a relative decrease in gene dosage, as the viral genome is replicated. In our design, we had sought to compensate this by using one of the strongest heterologous insect promoter (24), the immediate early 2 promoter from the multicapsid Nuclear Polyedrosis Virus of

Orgyia pseudotsugata (POpIE2), to drive *ns* expression. As insufficient expression of NS functions would effect inefficient replication rather than its complete shutdown, we conjectured that the observed defect could rather stem from an ineffective expression pattern linked to the absence of appropriate regulatory signals in the heterologous promoter sequence. To explore this hypothesis, we tested three different constructs in which POpIE2 was replaced by *i)* the 185 nucleotides (nts) immediately upstream of *ns3*'s start codon (core P93 promoter); *ii)* a larger fragment spanning 333 nts upstream (extended P93 promoter); and *iii)* a larger fragment of 595 nts (full upstream sequence missing the left end of the terminal hairpin). None of these modifications remediated the impaired replication phenotype (data not shown).

We next used a complementation strategy to determine whether the defective non-propagatable clone could be rescued in *trans*. Co-transfection with the infectious JcDV clone was indeed able to restore replication (Figure 2, p14). Likewise, a construct in which ITRs have been clipped down to the core P9 and P93 promoters was capable of functional rescue (Figure 2, p92). Since such a clone cannot replicate, this result disproves the potential implication of a replication-related disbalance in *ns* gene dosage. A truncated clone comprising only the *ns* gene block driven by its core promoter could not rescue replication (Figure 2, p90), further indicating that the replication defect is not directly related to NS functions. Instead, we found that complementation with the *vp* gene block only was sufficient to restore replication (Figure 2, p95). This result was particularly surprising, as capsid genes were not known to be involved in JcDV's replication process.

The rescuing *vp* block differs from the sequence in our defective non-propagatable clone by the presence of 99 nts from the natural sequence context downstream of the *vp* gene. We thus trimmed that region to test complementation by a *vp* gene block comprising only 33 additional nts, and found that it was not sufficient for rescue (Figure 2, p93). To confirm and extend these results, we constructed two amended versions of the defective clone in which the *vp* block is extended by 99 and 75 nts, respectively (Figure 2, p103-4). Both are capable of independent replication and represent functional non-propagatable clones that behave as originally intended (Figure 1D and Supplementary Figure 2).

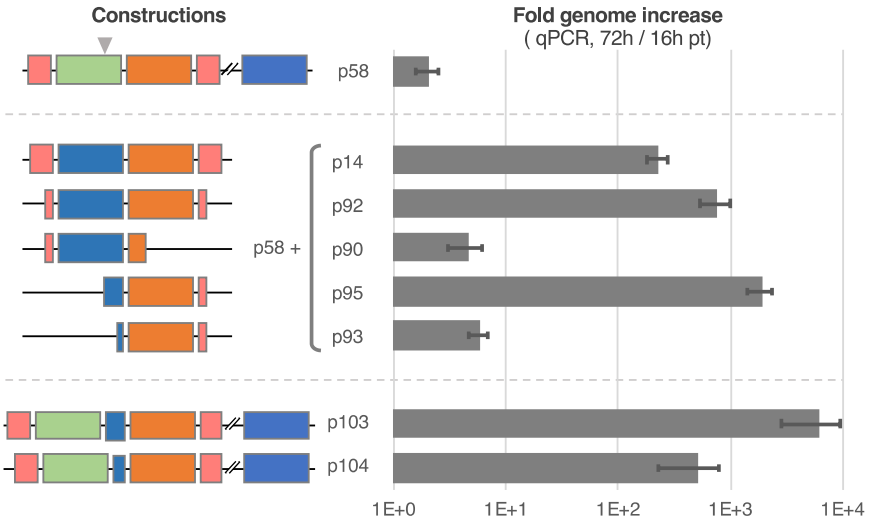

Figure 2 – Impaired replication of the defective clone is rescued by *vp* complementation

Shown are fold changes in genome quantity due to replication between 16h and 72h post-transfection of Ld652Y cells with various constructs, as measured by qPCR (grey arrowhead). For clarity, schematics of the constructs are shown on the left (red: *ITRs*; blue: *ns*; orange: *vp*; green: *reporters*). The original design of the non-propagatable genome (top, p58) shows almost complete absence of replication. Co-transfection with plasmids containing various fragments of the WT JcDV clone (left panel) permits to map the region necessary and sufficient for rescue. Both the WT genome (p14) and an ITR-less derivative (p92) complement the defective clone, while a fragment restricted to the *ns* gene block does not (p90). A large *vp* block comprising 115 nts downstream of the *vp* coding sequence (p95) effects high rescue level, while a fragment restricted to 49 nts of downstream context (p93) do not rescue at all. Extension of *vp*'s native downstream context from 16 (p58) to 91 nts (p104) or 115 nts (p103) yields increasingly more functional non-propagatable clones that function as originally intended (Supplementary Figure 2).

Transcript antisense interactions may repress replication but do not explain the role of vp

Although the results above readily fixed the faulty original design, they brought forward an unexpected role for the sequence region downstream of the *vp* coding sequence. Consequent to its ambisense genome architecture, JcDV's *ns* and *vp* transcripts antisense overlap by 60 nts on their respective 3' sides, with *vp*'s 3'UTR overlapping the *ns1* coding sequence by 44 nts (Figure 1A). As already noted for PCR polymerases, parvoviruses' terminal hairpins are not well processed by bacterial polymerases either. This creates recombinogenic conditions that render plasmid clones

unstable during propagation and amplification in bacteria. This issue is particularly marked with JcDV's long and stable hairpins (130 nts). In our original design, we had therefore opted to truncate *vp*'s 3'UTR by 59 nts in order to avoid introduction of recombination-prone sequence duplications (Figure 1B).

We reasoned that the absence of transcript overlap could prevent replication if an antisense regulation mechanism was somehow involved in upregulating *ns* expression (3, 21). To investigate whether base-pairing of the two transcripts is necessary for replication of the viral genome, we adopted a complementation strategy that enable independent manipulation of the antisense region on each transcript. We produced two sets of variants with 7 and 12 substitutions that are silent for NS1 while avoiding alteration of putative poly-adenylation signals (Figure 3A), and tested the effects of combining these sequences on the replication of a reporter construct.

Our results demonstrate sizable impacts of the substitutions, with up to 7-fold difference in replication efficiency (Figure 3B). However, the mechanism portrayed by our data is more complex than expected, with matching mutations displaying contrasted effects on the *ns* or *vp* blocks (Figure 3C). Substitutions in *ns* are associated with increased replication, unless they are complemented by matching *vp* mutations, which suggests that antisense regulation normally limits the expression of *ns* genes. Nonetheless, antisense mismatches driven by corresponding substitutions in *vp* hardly impact replication, supporting the notion that *vp* mutations exert some negative impacts on replication, which could compensate disruption of antisense regulation. Further supporting the existence of antisense regulation, we found that the number of mismatches between pairs of variants is associated with their statistical interactions (*i.e.* how much their joint impact is different from expectations based on their individual effect on replication, Figure 3D). According to this analysis, the missing *vp* region in our original construct does not impair replication by repressing *ns* expression, since the absence of antisense regulation would rather increase replication.

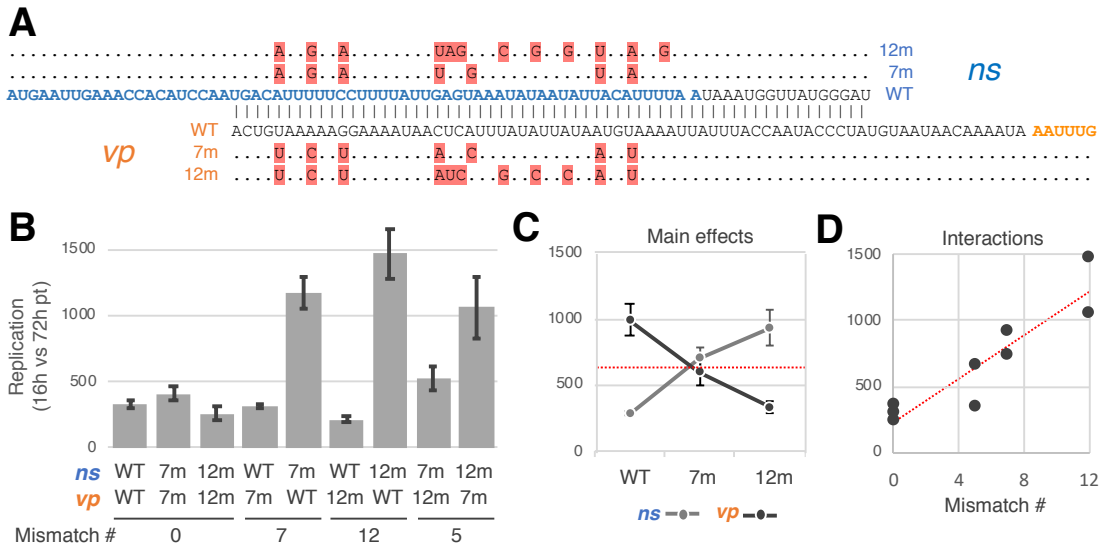

Figure 3 – Antisense transcript interactions do not explain *vp*'s impact on replication

A. Alignments of WT and mutated transcripts in the overlapping region between *ns* and *vp*. Complementary WT transcript sequence are shown in the middle. *ns* and *vp* coding sequences are colored in blue and orange, respectively. Transcript complementarity due to ambisense overlap is marked with vertical bars. Complementary mutations (7 or 12) were independently introduced in distinct *ns* and *vp* constructs. Mutations (highlighted in red) correspond to synonymous *ns1* substitutions and putative polyadenylation signals (green) are avoided. Dots convey sequence identity. **B.** Mutations in *ns* and *vp* transcript show moderate but complex effects on replication. Shown are fold change in genome abundance as measured by qPCR between 16 and 72h post-transfection of Ld652Y cells by the indicated plasmid pairs. Error bars show standard errors across 3 biological replicates. While complementary mutations have little net impact on replication, mismatches show largely different effects on *ns* or *vp* transcripts. **C.** Contrasted effects of complementary mutations on *ns* and *vp*. Shown is the marginal mean fold change in genome abundance over the 3 assays involving each construct. Error bars show standard errors over 9 biological replicates. In line with antisense regulation of *ns,* mutations affecting the *ns* transcript tend to increase replication. Symmetrical mutations in the *vp* transcript show opposite effects, hinting at a distinct mechanism. **D.** Transcript mismatches modulate mutational effects. Shown are absolute values of interactions between constructs against the number of mismatches between *ns* and *vp* transcripts. Interactions represent the difference between measured fold changes and

predictions based on main mutation effects plotted in panel C. Modulation by transcript mismatches confirms a role for antisense regulation.

vp's full 3'UTR is required for replication and determined by downstream sequence context

So far, we have shown that the 43 nts region extending from position +50 (p93) to +92 (p104) after *vp*'s stop codon is strictly required for replication (Figure 2). The most apparent functional features in this region are the polyadenylation (polyA) signal and site of *vp*'s transcript (Figure 1), respectively located at position +57:+62 and +75 (21). As mutating the *vp* transcript between these positions appear to negatively impact replication (Figure 3C), we sought to determine whether production of a complete *vp* transcript would be sufficient for rescue.

We constructed a *vp* block truncated just after the polyA site (p118) and found that it is not capable of supporting replication in previous complementation assay, yielding replication level similar to that of the shorter p93 (Supplementary Figure 3). We next performed 3'RACE to verify the exact position of *vp*'s polyA tail. The polyA site was conform to previous report (21) in both the WT clone and a functional *vp* block (p91, Figure 4A). In contrast, the transcript produced by the non-functional p118 block is shortened by 17 nts.

Molecular signals determining polyadenylation are known to be largely context dependent. In particular, T- or GT-rich downstream sequence elements (DSE) have been shown to play an important role in some instances (25). We thus carried a bioinformatic analysis of JcDV's genome and identified a local %GT peak just downstream of *vp*'s polyA site that is diminished in the sequence context of p118 (Figure 4B).

Altogether, these data show that production of a native *vp* transcript with full-length 3'UTR is essential for effective replication and might depend on a GT-rich downstream sequence to suppress a cryptic, upstream polyA signal.

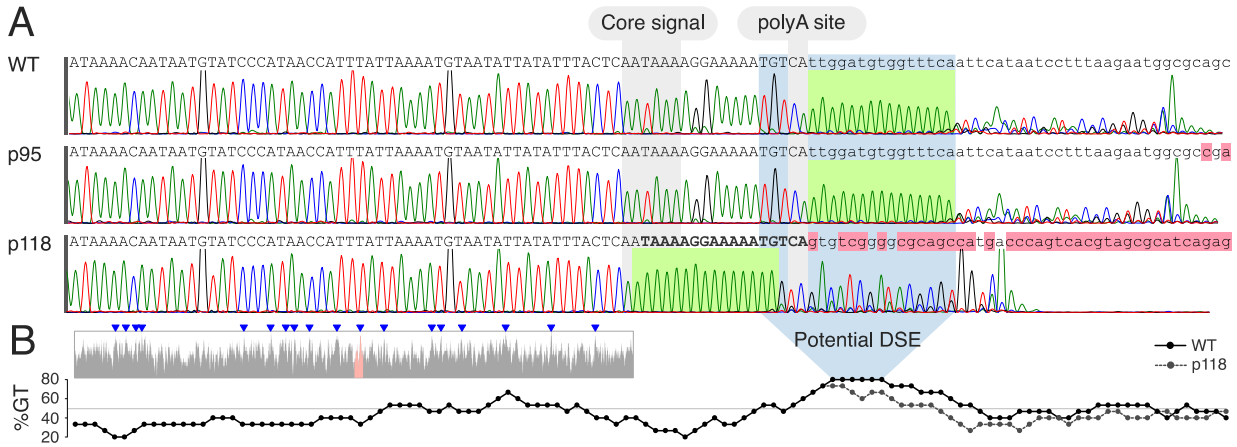

Figure 4 – Full *vp* 3'UTR is required for replication and specified by its immediate downstream context.

A. Impaired replication is associated with truncated 3'UTR. Shown are representative chromatograms of the sequence downstream of *vp*'s stop codon as obtained by 3'RACE. The sequence corresponding to each construct is shown on top. Mismatches (red background) correspond to the sequence context of the plasmid backbone. A construct comprising 115 nts of native context (p91) produce the same transcript as the WT clone. A construct truncated just after the polyA site (p118) produces shorter transcripts that lack the last 17 nts (bold) of the native 3'UTR and do not support replication (Supplementary Figure 3). **B.** Identification of a potential Downstream Sequence Element (DSE). The inset shows the %GT calculated for sliding windows of 15 nts over JcDV's genome. Blue arrowheads mark 18 peaks with %GT≥80. The red region correspond to the sequence shown in panel A and is enlarged in the main plot, where points show the %GT of sliding windows centered at these positions. The %GT peak located immediately downstream of the polyA site represents a potential DSE (solid line) that is largely attenuated in the p118 construction (dashed line).

VP's 3'UTR control VP but not NS expression

To further investigate the mechanistic link between *vp* transcript and replication, we sought to determine potential feedbacks of altered *vp* expression on *ns* expression. We first quantified the abundance of *ns* and *vp* transcripts using reverse transcription quantitative PCR (RT-qPCR). To avoid confounding gene dosage effects linked with differential replication, samples were collected

12h after transfection *i.e.* before any sizable replication can be detected (17). Cells transfected by the defective version of the non-propagatable clone (p58) show a 100-fold decrease in *vp* transcripts as compared to cells transfected with an amended functional version (p103). In sharp contrast, *ns* transcript abundances are identical in both background (Figure 5A). We conclude that truncation of *vp* transcript's 3'UTR results in its markedly decreased abundance, but does not appears to impact the *ns* transcript.

We next used immunofluorescence microscopy to quantify protein abundances and identify potential post-transcriptional regulations. To avoiding confounding replication effects while allowing sufficient time for protein synthesis, we co-transfected cells with combinations of non-replicative *ns* and *vp* blocks and quantified consequent VP, NS1 and NS2 signals 3 days post-transfection. Consistent with RT-qPCR data, we found that a construct yielding truncated *vp* transcripts leads to markedly lower VP protein abundances (Figure 5B). Co-transfection with the *ns* block results in a modest 1.8-fold increase in overall VP signal from the non-functional *vp* block and in a slight 1.3-fold decrease for the functional *vp* block (Figure 5B, right). Nonetheless, high VP-producing cells in the latter are clearly shifted toward higher production, with a 1.4-fold increase in the higher distribution mode (Figure 5B, left). This discrepancy might reflect differential co-transfection efficiencies. In any case, the presence of NS proteins does not appear to have a dramatic impact on VP expression. Similarly, our data does not suggest a strong impact of either native nor non-functional *vp* blocks on the expression levels of NS1 or NS2 (Figure 5C). These data were further confirmed by traditional western blots (Supplementary Figure 4C).

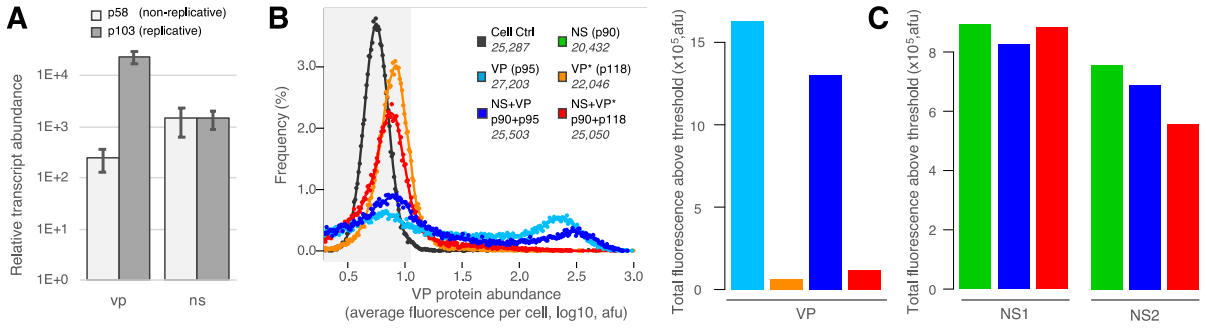

Figure 5 – Alteration of *vp*'s 3'UTR impacts VP but not NS expression.

A. Shorter 3'UTR decreases *vp* transcript abundance. Shown are relative transcript abundances, as quantified by RT-qPCR 12h after transfection of Ld652Y cells by the indicated plasmids. A functional version of the non-propagatable clone (p103, light grey) produces native *vp* transcript that cumulates to a 100-fold higher level than truncated transcripts from the defective clone (p58, dark grey). Abundances of *ns* transcripts are identical for both constructs. **B.** Shorter 3'UTR decreases VP protein abundance. Histograms (left) shows distributions of cellular fluorescence intensities, as quantified by immunofluorescence microscopy for VP proteins 3 days after transfection of Ld652Y cells by different combination of *vp* and *ns* blocks, as shown. Numbers indicate the number of analyzed cells. Data points represent cell frequencies over each percentile of the fluorescence range. For visual clarity, points are underlaid with loess regression smoothers. The 99_{th} percentile of control cells (grey background) is used as a threshold to quantify positive fluorescence signals. Barplot (right) shows the sum of fluorescence intensities for cells above threshold. Consistent with lower abundancies (panel A), truncated *vp* transcripts lead to strongly reduced VP protein level, both in the absence and presence of *ns* genes. **C**. Reduced VP expression has little impact on NS expression. Shown are barplots of total fluorescence intensities calculated as in panel B for cells marked for NS1 and NS2, respectively (Supplementary Figure 4AB). VP is not involved in upregulating NS expression.

Altogether, our results demonstrate that neither the nature of *vp*'s transcripts nor their differential consequences on VP protein abundances impact *ns* genes' expression. Thus, the impact of VP's 3'UTR on replication does not appear to involve any theretofore unknown feedback on NS regulation at either transcriptional and translational level. Instead, our data strongly suggest a more direct and essential role in replication for VP proteins, which is prevented by markedly lower protein expression from transcripts with truncated 3'UTR. To further verify this, we constructed two variants of the functional non-propagatable clone p103. In one, we substituted a nucleotide at position 1,626 of the 2,433 nts-long *vp* coding sequence to introduce a stop codon (p175). In the other, we deleted a nucleotide at position 2,061 to produce a frameshift (p183). Both of these clones were unable to support replication (Figure 6), unambiguously confirming the direct involvement of VP capsid protein in the replication of JcDV.

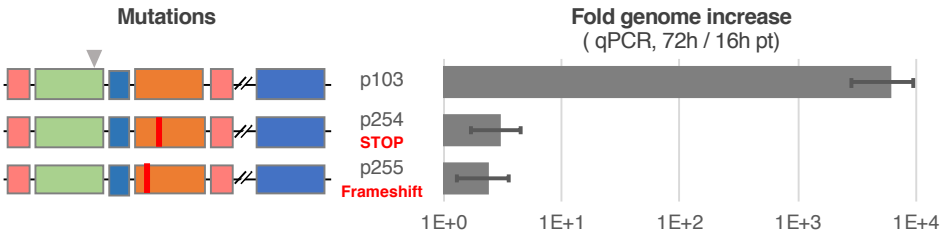

Figure 6 – VP proteins are directly involved in replication.

Shown are fold changes in genome quantity due to replication between 16h and 72h post-transfection in Ld652Y cells, as measured by qPCR (grey arrowhead). Data for p103 are reported from Figure 2 for comparison. Truncating VP proteins by introducing a stop codon (TA**T**|542|TA**G**; p254) or a frameshift (AA**T**|687|AA-, p255) abolishes replication. These mutations, which involve minimal DNA sequence modification and are separated by 435 nts, strongly support the link between VP proteins and replication.

DISCUSSION

We developed an efficient Golden Gate cloning strategy to precisely alter otherwise hard-to-manipulate parvovirus genomes (Supplementary Figure 1). We used this approach to genetically dissociate the capsid and non-structural gene clusters of the insect parvovirus JcDV (Figure 1). To implement this genomic rearrangement, we initially chose to truncate the 3'UTR of the capsid gene, which naturally overlaps the non-structural cluster to be relocated. This led us to uncover a profound impact of the capsid gene products on the replication of this parvovirus (Figures 2, 5 and 6).

We have shown that the region immediately downstream of *vp*'s polyA site is necessary to suppress an upstream polyA signal. This region likely comprises a GT-rich Downstream Sequence Element (DSE) that modulate polyadenylation (Figure 4B). Although more work is required to delineate the exact boundaries of this element, our data suggest that it functions in a cumulative fashion, with longer downstream sequences associated with stronger effects on replication (e.g. p103 vs p104, Figure 2).

In the absence of the putative DSE, a cryptic polyA site yields an alternate transcript species that is 17 nts shorter than the WT (p118, Figure 4A). This shorter 3'UTR determines markedly

decreased *vp* transcript abundances and VP proteins production (Figure 5AB and Supplementary Figure 4C), and is associated with an almost complete absence of replication (Supplementary Figure 3). The last 17 nts of the native 3'UTR may contain binding motifs for proteins that increase transcript stability, thus enabling higher protein production from more abundant transcript. Alternatively, regulatory proteins binding to such motifs could promote translation through RNA looping, and increased transcript stability would arise as a consequence of more active translation (26). We were, however, unable to identify known binding motifs in this region (27). Instead of sequential motifs, some RNA binding proteins recognize structural signals (28). *In silico* prediction shows that the end of the native 3'UTR can fold into a convincing secondary structure that exhibit a central bulge typical of such signals (29; Supplementary Figure 5A). The lower stem of that structure cannot form in the truncated transcript, due to the deletion of the corresponding sequence (Supplementary Figure 5B). In *vp*'s 3'UTR variants for which we identified potential negative impacts on replication (Figure 3), the cryptic polyA site is mutated and the predicted secondary structure is weakened to various extents (Supplementary Figure 5CD). Although regulatory proteins known to bind secondary structures in the 3'UTR usually inhibit translation, the structure at the end *vp*'s transcript could be involved in translation activation or, possibly, increased stability.

Regardless of the actual mechanism, the decrease in VP protein production due to premature transcript termination causes a dramatic and unexpected shutdown of viral replication. We found no evidence of strong *trans* expression feedbacks between VP and NS proteins, as has been documented for other parvoviruses (30-36). In particular, the impact of decreased abundance in *vp* transcript and VP proteins on replication does not appear to involve a direct effect on NS1 or NS2. While the precise role of NS2 is unknown, NS1 possesses nickase and helicase activities that are essential for rolling hairpin replication (22, 37). Although NS3 is also known to be essential for JcDV's replication, we could not investigate its expression pattern in this study for an effective cognate antibody is lacking (38). Nonetheless, we surmise that NS3's expression is highly unlikely to be impacted by VP. Indeed, both NS1 and NS2 are translated from transcripts spliced of *ns3* in such a way that all these genes present an almost identical 5'UTRs (Figure 1A; 21). Since VP proteins have little effect of the production of NS1-2, it is reasonable to infer that they do not

impact splicing and thus have no little effect on any splicing- nor 5'UTR-related regulations of *ns3*'s expression.

Our data suggest an essential role for VP proteins in the replication process of JcDV (Figure 6), through a mechanism that involves either protein interactions with NS proteins or autonomous replicative function for isolated VP proteins, their capsomeres or entire capsids. A few reports on other parvoviruses have pointed in these directions. For example, it was shown that combined mutations in VP2 of the mink enteritis parvovirus can diminish genome replication by up to 10 fold (39). A similar decrease in replication efficiency was also associated with VP2 mutations in porcine parvovirus (PPV; 40). As potential impacts on *ns* regulation were not tested in these studies, it is however difficult to conclude on the exact role played by these VP proteins.

More interestingly, replication of Adeno-Associated Virus Type 2 (AAV-2) and derivative recombinant genomes used in gene therapy was shown to stall to very low levels in the absence of efficient packaging (41). Both encapsidation and elongation levels were further found to be higher when the capsid gene (*cap*) is provided in *cis* rather than in *trans* of the packaged genome. These observations suggest a tight spatio-temporal coupling between replication, capsid protein expression and encapsidation. It was later elegantly confirmed that the formation of AAV-2 virions preferentially involves capsid proteins that are physically produced from the very genome that is packaged (9). Similar couplings have been described for positive-strand RNA viruses (42). Although the exact mechanistic basis of this process remains unknown, our observations that deficient VP expression or truncated proteins prevent replication and can be partially rescued by *trans* complementation are compatible with such a phenomenon. It is thus tempting to speculate that the dependency of replication over packaging could be a shared feature of parvoviruses.

All icosahedral viruses define a limited inner capsid volume that impose strong constraints on the upper size of the packaged genome (43, 44). From an evolutionary perspective, these constrains can be accommodated either physically—by increasing the capsid triangulation number to fit a larger genome or parting the latter into multiple capsids (multipartism); or informationally—through genetic information compression (*e.g.* overlapping genes). While multipartism could participate in increasing viral modularity (45), informational compression might create functional

dependencies between seemingly independent blocks that could greatly diminish it. Our observation that some function coded in the *vp* block is absolutely required for viral genome replication initially led us to question the effective modularity of JcDV's architecture, and more broadly of other parvoviruses and viruses. Our investigations did not permit to establish the precise mechanism underlying this dependency. If, as suggested above, this mechanism involves efficient packaging of the replicating genome rather than very specific interactions with NS proteins, that dependency may not in fact compromise modularity, nor its supposed evolutionary benefits in terms of evolvability. On the contrary, such a mechanism would prevent genome variants that are unable to produce propagatable capsid from depleting cellular resources via replication at the expense of other functional variants. This would also limit their hitchhiking functional capsids and enforce the genetic linkage between capsid variants and their corresponding genomes, thus facilitating the evolution of functional capsid variants.

SUPPLEMENTARY DATA

Supplementary Figures 1-5 and Supplementary Tables 1-2 are available with the online version of this article.

ACKNOWLEDGEMENTS

We are grateful to C. Clouet, M. Schatz and A.S. Gosselin-Grenet for useful discussions and technical assistance.

FUNDING

This work was partly funded by an individual MSCA fellowship grant to GC and an internal grant from the 'Santé des Plantes et Environnement' department of INRAE to GC.

CONFLICT OF INTEREST

The authors declare no conflict of interest.

REFERENCES

1. Koonin,E.V., Dolja,V.V. and Krupovic,M. (2015) Origins and evolution of viruses of eukaryotes: The ultimate modularity. *Virology*, **479-480**, 2–25.

2. Fakhiri,J., Schneider,M.A., Puschhof,J., Stanifer,M., Schildgen,V., Holderbach,S., Voss,Y., Andari,El,J., Schildgen,O., Boulant,S., *et al.* (2019) Novel Chimeric Gene Therapy Vectors Based on Adeno-Associated Virus and Four Different Mammalian Bocaviruses. *Molecular Therapy - Methods & Clinical Development*, **12**, 202–222.

3. Bergoin,M. and Tijssen,P. (1998) Biological and molecular properties of densoviruses and their use in protein expression and biological control. 10.1007/978-1-4615-5341-0_6.

4. Carlson,J., Suchman,E. and Buchatsky,L. (2006) Densoviruses for Control and Genetic Manipulation of Mosquitoes. *Adv. Virus Res.*, **68**, 361–392.

5. Tijssen,P. (1999) Molecular and structural basis of the evolution of parvovirus tropism. *Acta Vet. Hung.*, **47**, 379–394.

6. Allison,A.B., Organtini,L.J., Zhang,S., Hafenstein,S.L., Holmes,E.C., Parrish,C.R. and Ross,S.R. (2016) Single Mutations in the VP2 300 Loop Region of the Three-Fold Spike of the Carnivore Parvovirus Capsid Can Determine Host Range. *J. Virol.*, **90**, 753–767.

7. Multeau,C., Froissart,R., Perrin,A., Castelli,I., Casartelli,M. and Ogliastro,M. (2012) Four amino acids of an insect densovirus capsid determine midgut tropism and virulence. *J. Virol.*, **86**, 5937–5941.

8. Marsic,D., Govindasamy,L., Currlin,S., Markusic,D.M., Tseng,Y.-S., Herzog,R.W., Agbandje-McKenna,M. and Zolotukhin,S. (2014) Vector Design Tour de Force: Integrating Combinatorial and Rational Approaches to Derive Novel Adeno-associated Virus Variants. *Mol Ther*, **22**, 1900–1909.

9. Nonnenmacher,M., van Bakel,H., Hajjar,R.J. and Weber,T. (2015) High Capsid–Genome Correlation Facilitates Creation of AAV Libraries for Directed Evolution. *Mol Ther*, **23**, 675–682.

10. Ogden,P.J., Kelsic,E.D., Sinai,S. and Church,G.M. (2019) Comprehensive AAV capsid fitness landscape reveals a viral gene and enables machine-guided design. *Science*, **366**, 1139–1143.

11. Bossin,H. (1998) Développement de vecteurs d'expresssion stable dérivés du densovirus JcDNV : application à l'expression constitutive de protéines hétérologues en lignées cellulaires de lépidoptères et comme marqueur au cours du développement chez la drosophile.

12. Engler,C., Kandzia,R. and Marillonnet,S. (2008) A one pot, one step, precision cloning method with high throughput capability. *PLoS ONE*, **3**, e3647.

13. Lee,T.S., Krupa,R.A., Zhang,F., Hajimorad,M., Holtz,W.J., Prasad,N., Lee,S.K. and Keasling,J.D. (2011) BglBrick vectors and datasheets: A synthetic biology platform for gene expression. *J Biol Eng*, **5**, 12.

14. Pham,H.T., Huynh,O.T.H., Jousset,F.X., Bergoin,M. and Tijssen,P. (2013) Junonia coenia Densovirus (JcDNV) Genome Structure. *Genome Announcements*, **1**, e00591–13–e00591–13.

15. Kawaoka,S., Hayashi,N., Suzuki,Y., Abe,H., Sugano,S., Tomari,Y., Shimada,T. and Katsuma,S. (2009) The Bombyx ovary-derived cell line endogenously expresses PIWI/PIWI-interacting RNA complexes. *RNA*, **15**, 1258–1264.

16. Li,Y., Jousset,F., Giraud,C., Rolling,F. and Bergoin,M. (1996) A titration procedure of the Junonia cœia densovirus and quantitation of transfection by its cloned genomic DNA in four lepidopteran cell lines. *Journal of virological …*, 10.1016/0166-0934(95)01961-8.

17. Salasc,F., Mutuel,D., Debaisieux,S., Perrin,A., Dupressoir,T., Grenet,A.S.G. and Ogliastro,M. (2016) Role of the phosphatidylinositol-3-kinase/Akt/target of rapamycin pathway during ambidensovirus infection of insect cells. *Journal of General Virology*, **97**, 233–245.

18. Mutalik,V.K., Guimaraes,J.C., Cambray,G., Mai,Q.-A., Christoffersen,M.J., Martin,L., Yu,A., Lam,C., Rodriguez,C., Bennett,G., *et al.* (2013) Quantitative estimation of activity and quality for collections of functional genetic elements. *Nat. Methods*, **10**, 347–353.

19. Cambray,G., Guimaraes,J.C. and Arkin,A.P. (2018) Evaluation of 244,000 synthetic sequences reveals design principles to optimize translation in *Escherichia coli*. *Nat. Biotechnol.*, **54**, 198.

20. Goodwin,R.H., Tompkins,G.J. and McCawley,P. (1978) Gypsy moth cell lines divergent in viral susceptibility. I. Culture and identification. *In Vitro*, **14**, 485–494.

21. Wang,Y., Abd-Alla,A.M.M., Bossin,H., Li,Y. and Bergoin,M. (2013) Analysis of the transcription strategy of the Junonia coenia densovirus (JcDNV) genome. *Virus Res.*, **174**, 101–107.

22. Cotmore,S.F. and Tattersall,P. (2014) Parvoviruses: Small Does Not Mean Simple. *Annu Rev Virol*, **1**, 517–537.

23. Brandenburger,A., Coessens,E., Bakkouri,K.E. and Velu,T. (1999) Influence of Sequence and Size of DNA on Packaging Efficiency of Parvovirus MVM-Based Vectors. *Human Gene Therapy*, **10**, 1229–1238.

24. Bleckmann,M., Schürig,M., Chen,F.-F., Yen,Z.-Z., Lindemann,N., Meyer,S., Spehr,J. and van den Heuvel,J. (2016) Identification of Essential Genetic Baculoviral Elements for Recombinant Protein Expression by Transactivation in Sf21 Insect Cells. *PLoS ONE*, **11**, e0149424.

25. Proudfoot,N.J. (2011) Ending the message: poly(A) signals then and now. *Genes & Development*, **25**, 1770–1782.

26. Jacobson,A. and Peltz,S.W. (1996) Interrelationships of the Pathways of mRNA Decay and Translation in Eukaryotic Cells. *Annu. Rev. Biochem.*, **65**, 693–739.

27. Giudice,G., Sánchez-Cabo,F., Torroja,C. and Lara-Pezzi,E. (2016) ATtRACT-a database of RNA-binding proteins and associated motifs. *Database (Oxford)*, **2016**, baw035.

28. Szostak,E. and Gebauer,F. (2013) Translational control by 3'-UTR-binding proteins. *Briefings in Functional Genomics*, **12**, 58–65.

29. Mazumder,B., Poddar,D., Basu,A., Kour,R., Verbovetskaya,V., Barik,S. and García-Sastre,A. (2014) Extraribosomal L13a Is a Specific Innate Immune Factor for Antiviral Defense. *J. Virol.*, **88**, 9100–9110.

30. Rhode,S.L. and Richard,S.M. (1987) Characterization of the trans-activation-responsive element of the parvovirus H-1 P38 promoter. *J. Virol.*, **61**, 2807–2815.

31. Li,X. and Rhode,S.L.,III (1993) The Parvovirus H-1 NS2 Protein Affects Viral Gene Expression through Sequences in the 3′ Untranslated Region. *Virology*, **194**, 10–19.

32. Christensen,J., Cotmore,S.F. and Tattersall,P. (1995) Minute virus of mice transcriptional activator protein NS1 binds directly to the transactivation region of the viral P38 promoter in a strictly ATP-dependent manner. *J. Virol.*, **69**, 5422–5430.

33. Ward,T.W., Kimmick,M.W., Afanasiev,B.N. and Carlson,J.O. (2001) Characterization of the Structural Gene Promoter of Aedes aegypti Densovirus. *J. Virol.*, **75**, 1325–1331.

34. Raab,U., Beckenlehner,K., Lowin,T., Niller,H.-H., Doyle,S. and Modrow,S. (2002) NS1 Protein of Parvovirus B19 Interacts Directly with DNA Sequences of the p6 Promoter and with the Cellular Transcription Factors Sp1/Sp3. *Virology*, **293**, 86–93.

35. Aydemir,F., Salganik,M., Resztak,J., Singh,J., Bennett,A., Agbandje-McKenna,M. and Muzyczka,N. (2016) Mutants at the 2-Fold Interface of Adeno-associated Virus Type 2 (AAV2) Structural Proteins Suggest a Role in Viral Transcription for AAV Capsids. *J. Virol.*, **90**, 7196–7204.

36. Xu,P., Yuan,H., Yang,X., Graham,R.I., Liu,K. and Wu,K. (2017) Structural proteins of Helicoverpa armigera densovirus 2 enhance transcription of viral genes through transactivation. *Arch Virol*, **162**, 1745–1750.

37. Ding,C., Urabe,M., Bergoin,M. and Kotin,R.M. (2002) Biochemical Characterization of Junonia coenia Densovirus Nonstructural Protein NS-1. *J. Virol.*, **76**, 338–345.

38. Abd-Alla,A., Jousset,F.-X., Li,Y., Fédière,G., Cousserans,F. and Bergoin,M. (2004) NS-3 protein of the Junonia coenia densovirus is essential for viral DNA replication in an Ld 652 cell line and Spodoptera littoralis larvae. *J. Virol.*, **78**, 790–797.

39. Mao,Y., Su,J., Wang,J., Zhang,X., Hou,Q., Bian,D. and Liu,W. (2016) Roles of three amino acids of capsid proteins in mink enteritis parvovirus replication. *Virus Res.*, **222**, 24–28.

40. Fernandes,S., Boisvert,M. and Tijssen,P. (2011) Genetic Elements in the VP Region of Porcine Parvovirus Are Critical to Replication Efficiency in Cell Culture. *J. Virol.*, **85**, 3025–3029.

41. Ward,P., Clément,N. and Linden,R.M. (2007) cis Effects in Adeno-Associated Virus Type 2 Replication. *J. Virol.*, **81**, 9976–9989.

42. Saxena,P. and Lomonossoff,G.P. (2014) Virus Infection Cycle Events Coupled to RNA Replication. *Annu. Rev. Phytopathol.*, **52**, 197–212.

43. Wu,Z., Yang,H. and Colosi,P. (2009) Effect of Genome Size on AAV Vector Packaging. *Mol Ther*, **18**, 80–86.

44. Cui,J., Schlub,T.E. and Holmes,E.C. (2014) An Allometric Relationship between the Genome Length and Virion Volume of Viruses. *J. Virol.*, **88**, 6403–6410.

45. Lucía-Sanz,A. and Manrubia,S. (2017) Multipartite viruses: adaptive trick or evolutionary treat? *npj Syst Biol Appl*, **3**, 1–11.

46. Kerpedjiev,P., Hammer,S. and Hofacker,I.L. (2015) Forna (force-directed RNA): Simple and effective online RNA secondary structure diagrams. *Bioinformatics*, **31**, 3377–3379.

SUPPLEMENTARY DATA

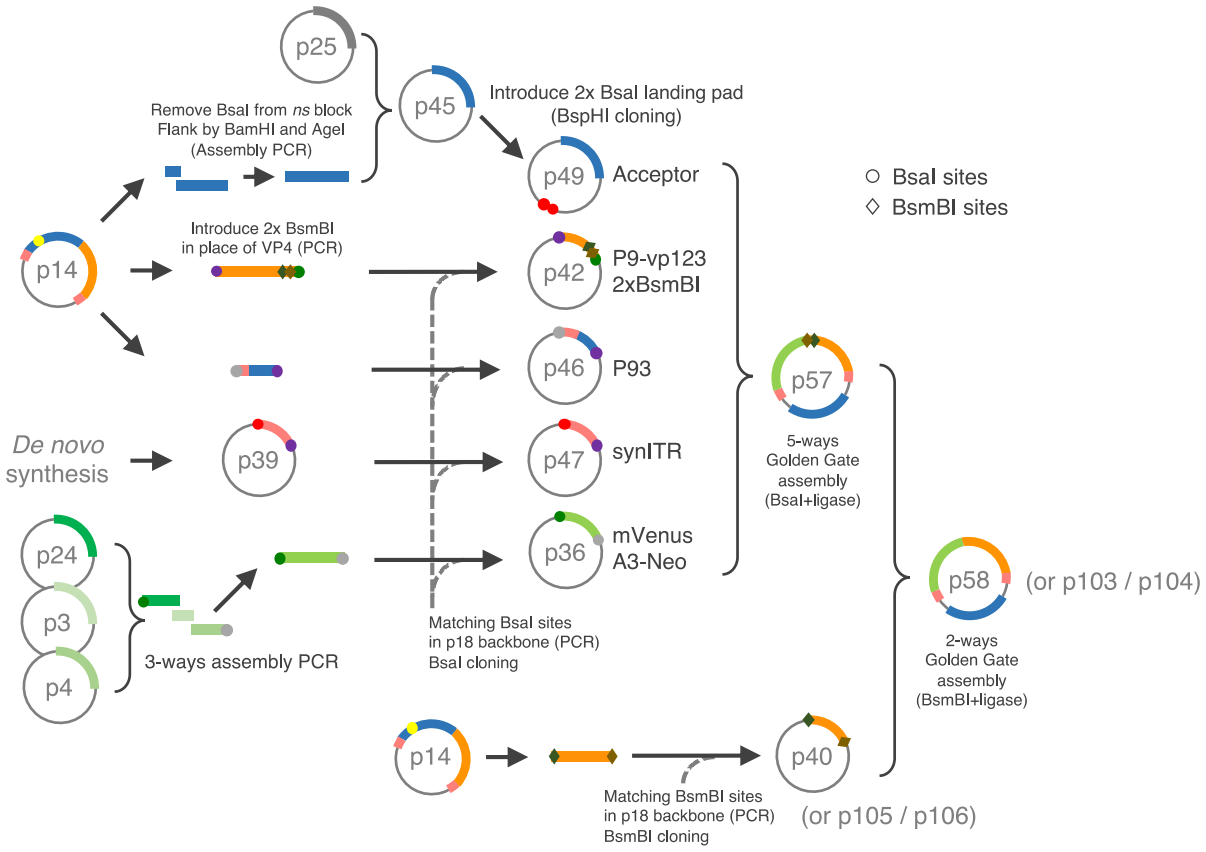

Supplementary Figure 1 – Efficient Golden Gate cloning strategy for precise modification of parvovirus genomes

The *ns* block—modified to erase a naturally occurring BsaI site—is cloned along with a double BsaI landing to form an acceptor plasmid (p42). Individual building blocks are flanked by BsaI sites by PCR, cloned in donor plasmids and sequence verified (p46, p47 and p36). A five-ways Golden Gate assembly of donor and accepting plasmid led to efficient assembly of the designed genome with a single reaction (p57). The order of assembled fragments is coded in the overhangs created upon BsaI digest (colored circles). Aside from the plasmid containing the PCR-refractory terminal hairpin (p39), all donor plasmids are easily amenable to modification by site directed mutagenesis. Because the original intent was to easily introduce mutation in *vp4*, this fragment was designed to be cloned in a final BsmBI Golden Gate cloning step into a *vp4*-less intermediate

acceptor construct, yielding the final construct (p58). The original *vp4* fragment (p40) was latter extended by site directed mutagenesis to increase the length of the 3'tail (p105 and p106) and yield functional non-propagatable clones (p103 and p104).

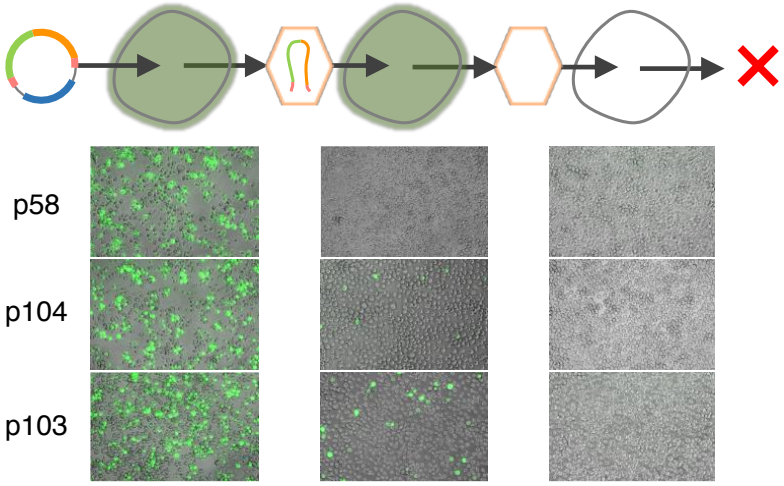

Supplementary Figure 2 – Amended versions of the non-propagatable clone function as intended

Images where taken using a regular DSLR camera fitted to an epifluorescence microscope. The first column shows Ld652Y cells 3 days post-transfection with different plasmid as shown. The second column show naïve cells 3 days post-transduction with 100 uL of clarified supernatant obtained from lysing transfected cells by repeated heat shock at 7 days pt. The third column show naïve cells 3 days post-transduction with 100 uL of clarified supernatant obtained from lysing first-round infected cells by repeated heat shock at 7 days pt. While no fluorescence could be observed for the first round of infection with the non-functional p58 construct, transduction was effective for the amended p104 and p103, to an extent commensurate with observed replication levels (see Figure 2). The second round of infection shows no signs of transduction, as expected from non-propagatable clones.

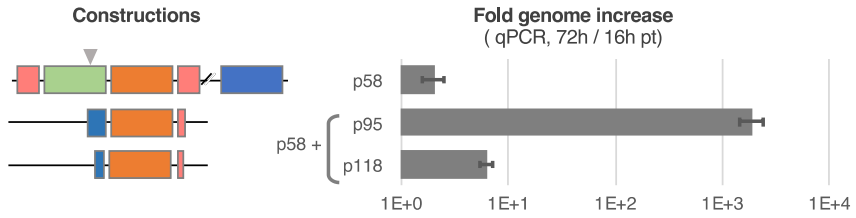

Supplementary Figure 3 – VP block truncated just downstream of the polyA site does not rescue replication.

Shown are fold changes in genome quantity due to replication between 16h and 72h post-transfection in Ld652Y cells, as measured by qPCR (grey arrowhead). Data for p58 and p58+p91 are reported from figure 2. Construct p118 corresponds to p91 truncated just after the CA of the polyA site (see Figure 4) and yields very low replication level when complementing p58.

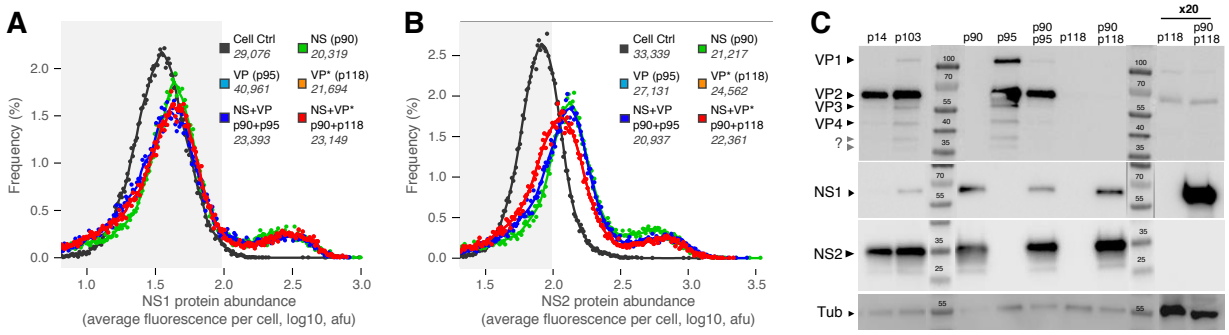

Supplementary Figure 4 – Alteration of *vp*'s 3'UTR impacts VP but not NS expression.

AB. Histograms show distributions of cellular fluorescence intensities, as quantified by immunofluorescence microscopy for NS1 (**A**) and NS2 (**B**) proteins 3 days after transfection of Ld652Y cells by different combination of *vp* and *ns* blocks, as shown. Numbers indicate the number of analyzed cells. Data points represent cell frequencies over each percentile of the fluorescence range. For visual clarity, points are underlaid with loess regression smoothers. The 99th percentile of control cells (grey background) is used as a threshold to quantify positive fluorescence signals. Barplots showing the sum of fluorescence intensities for cells above threshold are showed in Figure 5C. **C.** Shown are western blots for the same samples marked by different primary antibodies: anti-VP (top), anti-NS1 (middle-top), anti-NS2 (middle-bottom) and Tubulin (bottom). Samples are denatured total protein extracted from Ld652Y cell 3 days after

transfection with different plasmid combination, as indicated on top (p14 corresponds to the WT JcDV clone). All sample were diluted to the same extent, expect the last two lanes for which samples were diluted 20-fold less for comparison purposes. Protein species corresponding to each band are indicated by arrows on the right of the panel. Two additional species that are only visible in the highest concentrated samples of the VP blot are labeled with question marks and probably correspond to degradation products. Blot images were acquired using a chemiluminescence imager, and have been cropped to the signal of interest and individually adjusted for brightness and contrast. Ladders from bright field images were superimposed.

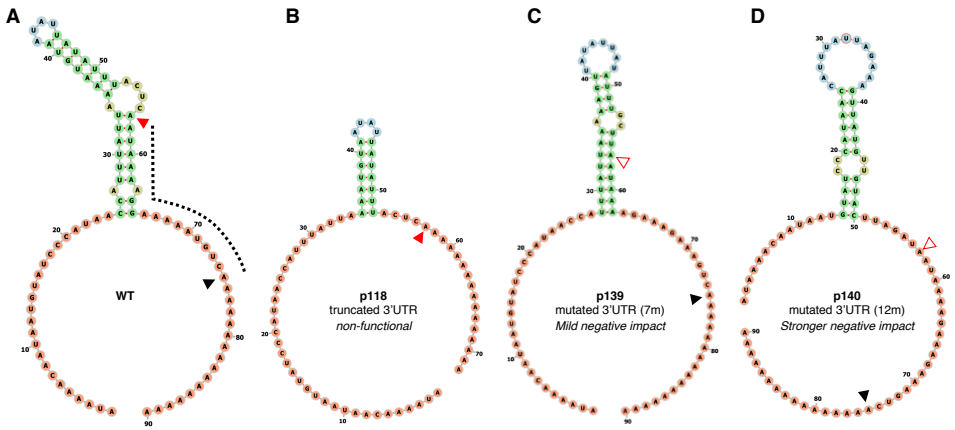

Supplementary Figure 5 – Potential structural binding site for regulatory protein in the 3'UTR of *vp*'s transcript.

A. Secondary structure prediction in the 3'UTR of *vp*'s native transcript. The 75 nts long 3'UTR was appended with a 15 nts polyA tail and folded. Bases are colored according to structural status. The sequence absents from early-terminated transcript that are non-functional for replication is highlighted with a dotted line: 8 nts are involved in the secondary structure. **B.** Secondary structure prediction in the 3'UTR of *vp*'s truncated transcript (from *e.g.* p118, Figure 4). The lower stem of the structure can no longer be formed. **CD.** Secondary structure prediction from *vp*'s 3'UTR mutants originally constructed to test antisense regulation. The 3'UTR is assumed to have WT length because the cryptic polyA site is mutated, though this was not verified experimentally. Mutations (7 and 12 in p139 and p140, respectively) results in increasingly altered secondary structures in both strength and position, which may reflect the increasingly negative impact on replication associated with these variants (Figure 3). Secondary structures were predicted using

the Vienna packages RNAfold webserver and rendered with FORNA (46). Black filled triangles mark the WT polyA, red filled triangle the cryptic polyA site and hollow red triangles mutated cryptic polyA site.

Supplementary Table 1 – Complete plasmids list

Full ID	*Name*	*Description*	*reference*
pGCDV1	pBRJH	Functional WT JcDV clone	11
pGCDV3	pITR-A3-GFP	*B. mori's* A3 actin promoter driving eGFP followed by SV40 polyA signals. Flanked by JcDV's ITR.	11
pGCDV4	pNeo	Contains neomycin resistance gene (neo)	Amersham
pGCDV10	pSB1C3::T7polymerase	Cloning backbone pSB1C3 with T7 polymerase insertion	iGEM DNA distribution (2014)
pGCDV14	pBRJH-CmR	WT JcDV clone derived from the original pBRJH clone	This work
pGCDV17	p15aCmR-eGFP-A3-Neo	Promoterless eGFP followed by SV40 polyadenylation signals and B. mori's A3 promoter driving *neo* gene.	This work
pGCDV18	pBbA2c-RFP	Minimal cloning backbone with p15a ori and chloramphenicol resistance	13
pGCDV24	mCerulean3-mVenus-FRET-10	A plasmid comprising mCerulean and mVenus coding sequences	addgene #58180
pGCDV25	pIZ-Flag6His-Siwi	pIZ backbone with Siwi gene insertion	15 (Addgene #50560)
pGCDV36	p15aCmR-mVenus-A3-Neo	Promoterless mVenus followed by SV40 polyadenylation signals and B. mori's A3 promoter driving neo gene. Flanked by BsaI sites.	This work
pGCDV39	pUC57-Kan-synITR_oxford	Extended ITR from oxford JcDV genome sequence synthesized by Genewiz and cloned in pUC57-Kan. Flanked by BsaI sites	14
pGCDV40	p15aCmR-vp4	JcDv's vp4. Flanked by BsmBI sites	This work
pGCDV42	p15aCmR-P9-vp123-2xBsmBI	JcDV's P9 and vp sequence excluding vp4 which is replace by two BsmBI accepting sites. Flanked by BsaI sites.	This work
pGCDV45	pIZ-ns-rmBsaI	pIZ backbone with ns gene block under POpEI-2 baculovirus promoter	This work
pGCDV46	p15aCmR_P93	JcDV's P93 promoter. Flanked by BsaI sites.	This work
pGCDV47	p15aCmR_synITR_oxford	Extended ITR from oxford JcDV genome sequence subcloned in p15a-CmR backbone. Flanked by BsaI sites.	This work
pGCDV49	pIZ-ns-BsaI_Lp	pIZ backbone with ns gene block under POpEI-2 baculovirus promoter and BsaI landing pad	This work
pGCDV55	pFAB217	A bacterial expression plasmid	18
pGCDV57	NoPropJcDV-venus-no_vp4	Original design of JcDV's non-propagatable clone. No vp4 sequence but BsmBI landing pad.	This work

pGCDV58	NoPropJcDV-venus-vp4-16_tail	Original (defective) design of JcDV's non-propagatable clone with 16 nts after vp's stop codon	This work
pGCDV73	NoPropJcDV-venus-vp4-Δns	A derivative of p58 in which the *ns* gene block is replaced by a 500+ nts DNA spacer	This work
pGCDV90	pJDvp	JcDv's P93 and *ns* followed by 484 nts after *ns1*'s stop codon	17
pGCDV91	pJDns	JcDv's P9 and *vp* followed by 115 nts after *vp*'s stop codon	17
pGCDV92	pJA	pBRJH derivative with truncated ITRs (no hairpin, no replication)	16
pGCDV93	pJDns_49_tail	JcDv's P9 and *vp* followed by 49 nts after *vp*'s stop codon	This work
pGCDV103	NoPropJcDV-venus-vp4-115_tail	Amended (functional) design of JcDV's non-propagatable clone with 115 nts after *vp*'s stop codon	This work
pGCDV104	NoPropJcDV-venus-vp4-91_tail	Amended (functional) design of JcDV's non-propagatable clone with 91 nts after *vp*'s stop codon	This work
pGCDV105	p15aCmR-vp4-115_tail	JcDv's vp4 followed by 115 nts after stop codons. Flanked by BsmBI sites	This work
pGCDV106	p15aCmR-vp4-91_tail	JcDv's vp4 followed by 91 nts after stop codons. Flanked by BsmBI sites	This work
pGCDV116	JcDV_Replication_reporter	JcDV's extended (oxford) ITRs flanking a DNA sequence of the same length as the WT genome. Comprises eGFP driven by *B. Mori*'s A3 promoter and followed by SV40 polyadenylation signal	This work
pGCDV118	pJDns-75_tail	JcDv's P9 and *vp* followed by 75 nts after *vp*'s stop codon (stops just after polyA site)	This work
pGCDV144	pJDns-7m_ns_recod	JcDv's P9 and *vp* followed by 115 nts after *vp*'s stop codon with 7 substitutions in the ns1 overlapping region	This work
pGCDV145	pJDns-12m_ns_recod	JcDv's P9 and vp followed by 115 nts after vp's stop codon with 12 substitutions in the ns1 overlapping region	This work
pGCDV146	pJDvp-7m_ns_recod	JcDv's P93 and ns followed by 484 nts after ns1's stop codon. 7 silent substitutions in the end of ns1	This work
pGCDV147	pJDvp-12m_ns_recod	JcDv's P93 and ns followed by 484 nts after ns1's stop codon. 12 silent substitutions in the end of ns1	This work
pGCDV252	p15aCmR-vp4_168tag-115_tail	JcDv's vp4 followed by 115 nts after stop codons and tat542tag substitution in *vp* (stop codon). Flanked by BsmBI sites	This work
pGCDV253	p15aCmR-vp4_314aa--115_tail	JcDv's vp4 followed by 115 nts after stop codons and aat687aa-deletion in *vp* (frameshift). Flanked by BsmBI sites	This work
pGCDV254	DefectJcDV-venus-vp4_168tag-115_tail	Amended design of JcDV's non-propagatable clone with 115 nts after *vp*'s stop codon and tat542tag substitution in *vp* (stop codon)	This work
pGCDV255	DefectJcDV-venus-vp4_314aa--115_tail	Amended design of JcDV's non-propagatable clone with 115 nts after *vp*'s stop codon and aat687aa- deletion in *vp* (frameshift)	This work

Supplementary Table 2 – Oligonucleotides

Full ID	*Sequence (5' -> 3')*

oGCDV6	CTGTTCGAGCACACCTTAGTAAATGATACATTGATGAGTTTGGACAAACCACAAC
oGCDV7	GTTGTGGTTTGTCCAAACTCATCAATGTATCATTTACTAAGGTGTGCTCGAACAG
oGCDV8	CAATCATGCGAAACGATCCTCATATTGTAACTTCTTCGTCGCACCTCTTG
oGCDV9	CAAGAGGTGCGACGAAGAAGTTACAATATGAGGATCGTTTCGCATGATTG
oGCDV14	AAGGTAAAGGGACGGAGAAC
oGCDV19	CATAAGGGTCACGATGGTTAATTAATTC
oGCDV20	TAACCATCGTGACCCTTATGATACTGATG
oGCDV37	CTCAGCCTACACACTTTCCA
oGCDV40	CGAAAATCCACAGATACAACCAAG
oGCDV41	GGGTTAGTATTAGCATCAGTCGAAAAT
oGCDV54	TTTGGTCTCAATGGTGAGCAAGGGCGAGGAGCTGTTC
oGCDV55	TTTGGTCTCATGTAATATTATATTTAGAAGAACTCGTCAAGAAGGCGATAG
oGCDV56	TTTTACAAGAGACCGGGCCTTTCTGCGTTTATAC
oGCDV57	TTTCCATAGAGACCGACGTTGATCGGCACGTAAG
oGCDV61	TTTTGAAGACTTACTTGTACAGCTCGTCCATG
oGCDV62	AAAAGAAGACACAAGTAAGCGGTCGACGCGTGCTAAG
oGCDV63	TTTTGAAGACCTCACCATAGAGACCGACGTTGATC
oGCDV64	GCAGTTCATTCAGGGCAC
oGCDV85	TTTTGTAAGAGACCGGGCCTTTCTGCGTTTATAC
oGCDV94	TTTGGTCTCATACATGAGACGCGTCTCATAGCCATTTCAACGTCAAGAGAAGTAG
oGCDV96	AGTACGTCTCATACATTATTGTTTTATTTAAACGTTACCAAG
oGCDV97	ATATACGTCTCGGCTATGTCATTACCTGGAACTGGTTC
oGCDV112	AAAAGGATCCTTGTGCAAAAGTGGTTCCAGAATATAATC
oGCDV113	ATATACCGGTCAATAATGTATCCCATAACCATTTATTAAAATG
oGCDV114	TTTTGGTCTCAAAACTCGCGTCGAGGCTGGGCCGTG
oGCDV115	TTATGGTCTCACCATTCTGGAACCACTTTTGCACAACAC
oGCDV116	TTTTTGTAAGAGACGGGGCCTTTCTGCGTTTATAC
oGCDV117	TATATTAGCAGAGACGGACGTTGATCGGCACGTAAG
oGCDV120	CATGTTGCGGAGACCTACGTACTGGTCTCGGCAA
oGCDV121	CATGTTGCCGAGACCAGTACGTAGGTCTCCGCAA
oGCDV122	TTTGCAAAGAGACCGGGCCTTTCTGCGTTTATAC
oGCDV127	TTTTGTTTAGAGACCGACGTTGATCGGCACGTAAG
oGCDV128	TTTTATGGAGAGACCGGGCCTTTCTGCGTTTATAC
oGCDV147	TTTTAAACTGAGACCGACGTTGATCGGCACGTAAG
oGCDV182	ATGGATTGCACGCAGGTTCT
oGCDV183	TTGCAGTTCATTCAGGGCAC
oGCDV223	GTGTCGGGGCGCAGCCATGACCCAGTCACGTAGCGATAG
oGCDV227	TCATGGCTGCGCCCCGACACTATAATATTACATTTTAATAAATGGTTATGGGATAC
oGCDV233	TTTTGGTCTCTTGGATGCGCGTTACCATATATGG
oGCDV234	CCAAGCACTAGTCATCCGGTAGCGATACATTGATGAG
oGCDV235	GCTACCGGATGACTAGTGCTTGGATTCTCACC
oGCDV236	AAAAGGTCTCATGGACACGGACAGAAAATTTGTGCCCAT
oGCDV239	TATAGGTCTCCTACATCGGCGCCATTCTTAAAGGATTATG
oGCDV243	ATATAGGTCTCGGCTATGTCATTACCTGGAACTGGTTC
oGCDV244	TATAGGTCTCCTACATTGAAACCACATCCAATGACATTTTTCC
oGCDV285	TCATGGCTGCGCCCCGACACTGACATTTTTCCTTTTATTGAGTAAATATAATATTAC
oGCDV295	TTCTTTTATTAAGCAAATATAATATAACTTTTTAATAAATGGTTATGGGATACATTATTG

oGCDV296	GTTATATTATATTTGCTTAATAAAAGAAAGAAAGTCATTGGATGTGGTTTC
oGCDV297	TTCTTTTATTATCTAAGTACAACATAACTTTCTAATAAATGGTTATGGGATACATTATTG
oGCDV298	GTTATGTTGTACTTAGATAATAAAAGAAAGAAAGTCATTGGATGTGGTTTC
oGCDV307	CACATGAAGCAGCACGACTT
oGCDV308	TCTGCTTGTCGGCCATGATA
oGCDV365	TTGTACGAAAACGGGGAGAG
oGCDV366	CTGCCAGCATCTGATCTACG
oGCDV393	AGTTATAGGTTCCTATTTTGGTGCACTAGTAGC
oGCDV394	GCACCAAAATAGGAACCTATAACTGGTACG
oGCDV395	TTAAACAAATTAGCTGGAAATTGCGAGTCAAATTATGAGTTGATTCAG
oGCDV396	CTCATAATTTGACTCGCAATTTCCAGCTAATTTGTTTAATATTTATTCTGAC